THE JOURNAL OF PHYSICAL CHEMISTRY B

Subscriber access provided by UNIV OF WISCONSIN - MADISON

B: Biomaterials, Surfactants, and Membranes

Polycation Interactions with Zwitterionic Phospholipid Monolayers on Oil Nanodroplets Suspensions in Water (DO) Probed by Sum Frequency Scattering

Laura L. Olenick, Julianne M. Troiano, Nikolay Smolentsev, Paul E. Ohno, Sylvie Roke, and Franz M. Geiger

J. Phys. Chem. B, **Just Accepted Manuscript** • DOI: 10.1021/acs.jpcb.8b00309 • Publication Date (Web): 24 Apr 2018

ACS Publications

is published by the American Chemical Society. 1155 Sixteenth Street N.W., Washington, DC 20036

Polycation Interactions with Zwitterionic Phospholipid Monolayers on Oil Nanodroplets Suspensions in Water (D_2O) Probed by Sum Frequency Scattering

Laura L. Olenick,[a] Julianne M. Troiano,[a#] Nikolay Smolentsev,[b] Paul E. Ohno,[a] Sylvie Roke,[b*] And Franz M. Geiger[a*]

[a]Department of Chemistry, Northwestern University, 2145 Sheridan Road, Evanston, IL 60208, USA, [#]now at the Department of Chemistry, Massachusetts Institute of Technology, 77 Massachusetts Avenue, 2-014, Cambridge, MA 02139, USA [b]Laboratory for fundamental BioPhotonics, Institutes of Bioengineering and Materials Science and Engineering, School of Engineering, and Lausanne Centre for Ultrafast Science, École Polytechnique Fédérale de Lausanne (EPFL), CH-1015 Lausanne, Switzerland.

*Authors to whom correspondence should be addressed: geigerf@chem.northwestern.edu and sylvie.roke@epfl.ch

Abstract. By combining dynamic light scattering (DLS) measurements with the interface- and bond-specificity of vibrational sum frequency generation scattering (SFS) spectroscopy, we probe several structural aspects of how zwitterionic DMPC lipids adsorbed to oil droplets suspended in water (D_2O) respond to the presence of the common polycation polyallylamine hydrochloride (PAH) in the presence of low and high salt concentration. We show that the polycation interactions with the lipids generally results in two distinct outcomes that depend upon salt and PAH concentration, identified here as Scheme 1 (observed under conditions of high salt concentration) and Scheme 2 (observed under conditions of low salt concentration). The Schemes differ in the extent of changes to droplet size and droplet coalescence coinciding with PAH addition. Our

combined DLS and SFS results illustrate that cationic polymers do not always interact in the same fashion with lipid membranes and demonstrate the feasibility of second-order spectroscopic methods to probe those interactions with chemical bond specificity, not only for the alkyl tails (C-H stretches) but also the choline headgroup (P-O stretches).

I. Introduction. Polycations are an important component of many chemical applications, where they are used, for instance, as ligands for engineered nanomaterials,[1] in drug delivery systems,[2] as anti-microbials,[3] and as additives in polymer resins used in consumer products.[4] While the benefits of polycations are numerous, these compounds also have the potential to be harmful once they enter the environment, as they may interact strongly with bacterial membranes even at relatively modest concentrations, as reported recently for the common polycation poly(allylamine hydrochloride) (PAH).[5-9] The interaction between another cationic polymer, poly(ethlenimine), and mouse fibroblast cells has been shown to induce necrotic cell death.[10] Similarly, polycation-DNA polyplexes have been reported to adhere to cells by interacting with negatively charged phospholipids in cell membranes,[11] while the polycationic bioadhesive chitosan has been reported to disturb the protective boundary of the outer membrane of Gram-negative bacteria.[12] In addition, cationic species coupled with complexes of adenovirus can modify the efficiency of gene transfer,[13] while the incorporation of hydrophilic spacers into polycations has been shown to improve gene delivery into targeted cells.[11] Understanding polycation-lipid interaction on the molecular level therefore provides an opportunity to identify pathways for chemically modifying polycations so that potentially negative biological outcomes may be avoided while technological benefits are maintained, or perhaps even improved.

While several approaches have been used to determine polycation-membrane interaction mechanisms on a molecular level, ascertaining the role of molecular structure in this line of research has been challenging. The broad molecular weight distributions of many polymers is one of the problems.[3] But, perhaps more importantly, the elucidation of interaction mechanisms by structural studies has been complicated by difficulties in applying label-free – yet chemically specific – probes to probe the relevant interfacial processes. Yet, some important insights have been gained. For instance, Banaszak-Holl and co-workers combined atomic force microscopy (AFM) and nuclear magnetic resonance spectroscopy to determine that polymer class and fluid phase state govern the interaction mechanism between polycationic polymer nanoparticles and lipid bilayers formed from the zwitterionic lipid 1,2-dimyristoyl-*sn*-glycero-3-phosphocholine (DMPC).[14] Likewise, Hong et al. used AFM and confocal laser scanning microscopy to identify the importance of polymer charge state in the formation of nanoscale holes within supported lipid bilayers exposed to polycations, while neutral polymers did not exhibit this effect.[15] Standard fluorescence techniques have also been used in permeability assays, quantifying leakage of fluorescent materials out of, or into, suspended vesicles exposed to cationic polymers.[12] Polycationic dendrimers have also been reported to bend anionic membranes, thus inducing stress and increasing vesicle leakage.[16] Similarly, Davydov et al. reported phase transition temperatures measured using differential scanning calorimetry that indicated structural changes within membranes exposed to polycations depend on lipid composition.[17] Finally, our own recent work combined nonlinear optical spectroscopy with molecular dynamics simulations to probe supported lipid bilayers interacting with PAH. This work identified considerable shifts in the pK_a values of the PAH ammonium groups, along with counterion condensation, as a means for building up considerable PAH surface coverages while mitigating charge-charge repulsion in the crowded

interfacial environment.[6] Direct ammonium-phosphate interactions were shown to be important in that study as well in that work.

Despite the abundance of research on polycation-lipid interactions, much remains to be discovered about the structural changes that occur in response to various stressors, and under conditions of varying ionic strength. Here, we combine dynamic light scattering (DLS) measurements with the interface- and bond-specificity of vibrational sum frequency generation (SFG) spectroscopy to probe several aspects of the molecular structure of lipid monolayers from DMPC lipids suspended in a liquid system composed of oil/water droplets. The lipid-coated droplets are exposed to varying concentrations of PAH in the presence of low and high salt concentration and studied using sum frequency scattering (SFS) spectroscopy,[18] which is uniquely suited for probing lipid membranes in suspensions rather than immobilized supports, for which SFG spectroscopy in a reflection geometry is amenable.[19-29] We show that polycation interactions with zwitterionic lipid bilayers generally result in two distinct outcomes that depend upon salt and PAH concentration, identified here as Scheme 1 and Scheme 2.

We selected PAH for these polymer–lipid membrane interaction studies due to its importance in studies involving lipid membranes,[30] cancer cells,[31] and organismal toxicity,[32] as well as its use as a common wrapping for nanomaterials.[33] DMPC was used in the present study because it has also been widely studied and contains the phosphatidylcholine (PC) headgroup, which is prevalent in the membranes of eukaryotes.[34-38] In order to probe PAH-DMPC membrane interactions, we used a membrane model system composed of phospholipid monolayers coating the surfaces of oil nanodroplets.[39] Since oil droplets are hydrophobic in nature, the phospholipid orients itself with the hydrophilic portion in the aqueous phase. The polycations introduced into the system then interact with the headgroups of the monolayer, much as they would with the

headgroups in a lipid bilayer. The oil droplets studied here possess controllable molecular interfacial properties[39] and have been previously used to study lipid structure and orientation as well as the interactions of the oil droplets with ions.[40]

When compared to lipid monolayers formed in a Langmuir trough, one advantage is that the current approach requires considerably smaller sample volumes, and that the lipid tails are in contact with a liquid hydrophobic phase rather than air.[39] In addition, recent experiments comparing micron- and nano-sized interfaces to extended planar interfaces have shown that the balance of interactions is different, which leads to different surface chemistry and interactions.[41-42] Eliminated final sentence here.

II. Experimental.

A. Chemicals. PAH was purchased from Sigma Aldrich (283215, ~17.5 kDa) and used without further purification (>95%). DMPC was purchased in powder form (>99%, Avanti Polar Lipids), stored at -20°C until use, and used without further purification. Sodium chloride (≥ 99%, Sigma Aldrich), d_{34}-hexadecane (98%, Cambridge Isotope Laboratories), and D_2O (99.8%, Armar Chemicals) were used as received.

B. Oil Droplet Preparation. In order to prepare nanoscale oil droplets (nanodroplets), powdered DMPC was hydrated in D_2O at a concentration of 2 mM for 30 minutes at approximately 40°C, ensuring that the hydration occurred above the transition temperature of the lipids (24 °C for DMPC).[43] Deuterated hexadecane was then added at 1 vol % to the hydrated DMPC suspension. The lipid-oil suspension in D_2O was sonicated for periods of five minutes at an intensity setting of 40% on the ultrasonic bath (35 kHz, 400 W, Bandelin sonorex digiplus) until a DLS size measurement indicated a polydispersity index (PDI) below 0.25 and a diameter between 100 and 200 nm. Once the sample met these criteria and the solution was milky white and homogeneous,

the sample was used for no more than one week, stored in the refrigerator. Sample stability was verified with DLS before each SFS measurement.

For SFS measurements, 60 μL of the nanodroplet solution was placed into a cuvette composed of a fused silica window with a slight interior indentation (Hellma Analytics, 106-0.20–40, Germany) and a detachable CaF_2 window (CeNing Optics, 1.3 mm thick, 60-40S/D, L/2). Care was taken not to trap air bubbles within the sample during preparation of the cuvette. The CaF_2 window was oriented towards the incoming IR and visible beams, and the quartz window was oriented towards the detector. All experimental data shown in the main text was obtained in duplicate. For SFS experiments in the CH stretching region, PAH solutions were made from PAH stock solutions composed of 41 mM PAH in 1 mM NaCl in D_2O. For SFS experiments in the PO stretching region, PAH solutions were made from PAH stock solutions composed of 2.3 mM PAH in 1 mM NaCl in D_2O. Aliquots of PAH stock solutions were added to the lipid oil droplet solutions via micropipette. Solutions were vortexed for ten seconds and then allowed to sit at room temperature for 20 minutes prior to SFS experiments.

Creaming can be easily detected during the experiment and did not occur on the time scale of the measurement. The sample is shaken before each measurement, i.e. it is well mixed prior to being placed in the cuvette. Once the solution is placed in the cuvette, the acquisition begins immediately. The sample is not shaken during SFG spectral acquisition.

C. SFS system. Vibrational SFS spectra were recorded using our previously described approach.[44-46] Briefly, an 800 nm regeneratively amplified 1 kHz Ti:sapphire system (Spitfire Pro, Spectra physics) was used to pump a HE-TOPAS-C (Light Conversion) optical parametric amplifier to generate IR pulses. The visible beam was split off directly from the amplifier and spectrally shaped with a home-built pulse shaper for a spectral resolution of 10 cm^{-1}. The angle between the 10 μJ

visible (VIS) beam (800 nm, FWHM 10 cm^{-1}) and the 6 μJ IR beam (9700 nm or 3200 nm, FWHM 160 cm^{-1}) was 20° (as measured in air). The IR and visible beams were focused using parabolic gold mirror with effective focal length of 101.6 mm (84-625, Edmund Optics) and plano-convex lens (LA1484-B, Thorlabs) overlapped in a sample cuvette with a path length of 200 μm at incident angles of 35° and 55°, respectively. At a scattering angle of 55° with respect to 800 nm beam, the scattered SF light was collimated using a plano-convex lens (f=15 mm, Thorlabs LA1540-B) and passed through two short wave pass filters (3rd Millenium, 3RD770SP). The SF light was spectrally dispersed with a monochromator (Acton, SpectraPro 2300i) and detected with an intensified CCD camera (Princeton Instruments, PI-Max3) using a gate width of 10 ns. The acquisition time for a single spectrum was 10-20 min for P-O stretch modes and 20 min for C-H stretch modes. A Glan-Taylor prism (Thorlabs, GT15-B), a half-wave plate (EKSMA, 460-4215), and a polarizing beam splitter cube (CVI, PBS-800-050), and two BaF_2 wire grid polarizers (Thorlabs, WP25H-B) were used to control the polarization of the SFG, VIS, and IR beams, respectively. The SFG and VIS beams were polarized in the vertical (S) direction and the IR beam was polarized in the horizontal plane (P) with respect to the plane of incidence, leading to the polarization combination $S_{out}S_{in}P_{in}$. The recorded intensity was baseline subtracted and normalized to the SFG spectrum obtained from a gold mirror in $P_{out}P_{in}P_{in}$ polarization and in a conventional reflection geometry (with incident angles of 45° for vis and 65° for IR) that was recorded before each measurement. Droplet size was accounted for by dividing the SFS spectrum by the radius of the droplet cubed (r^3), based on DLS data (the Z-average provided by the Zetasizer software size intensity distribution cumulant results found under the "Intensity Peak Stats" tab in the software), as described previously.[18] Daily changes in power were accounted for by dividing the SFS spectrum by the power (both IR and visible) multiplied by the acquisition time (in seconds).

D. Dynamic Light Scattering. Dynamic Light Scattering measurements utilized a Malvern Zetasizer Nano ZS. Each size result shown is the average of three measurements, each of which is the average of 11 data points. Standard deviation is calculated from the three replicates. All DLS data was acquired on the same samples that were used to acquire the SFS data.

III. Results and Discussion

III. A. PAH modifies SFS spectral intensity of DMPC/d-hexadecane nanodroplets depending on NaCl concentration. SFS spectra in the CH stretching region were obtained from DMPC/oil nanodroplets dispersed in D_2O, without added salt. The *ssp*-polarized spectra in the absence of salt (Figure 1A) include the symmetric methylene stretch (s-CH_2) near 2850 cm^{-1}, the symmetric methyl stretch (s-CH_3) near 2879 cm^{-1}, the antisymmetric methyl stretch (as-CH_3) near 2865 cm^{-1}, the antisymmetric methylene stretch (as-CH_2) near 2919 cm^{-1}, as well as the methylene Fermi resonance near 2905 cm^{-1} and the methyl Fermi resonance near 2937 cm^{-1}.[47-49] The spectra are comparable to those obtained from systems having similar hydrocarbon tails, such as those recently published by the Richmond group using similar methods.[50]

Upon interaction with a 140 μM solution of PAH the SFS signal intensity from the DMPC/oil nanodroplets decreases by approximately 60% in both the *ssp* and *ppp* polarizations (Fig. 1A and B). Size changes observed by DLS are negligible (*vide infra*). The relative SFG peak intensities remain the same, indicating that the orientation of the lipids with respect to the interface does not change notably in response to the presence of PAH under the conditions of this experiment.

Unlike the SFS spectra from DMPC/oil nanodroplets interacting with PAH under conditions of "no added salt", combining the nanodroplet solution with a solution of 140 μM PAH in 100 mM NaCl (~9 mS/cm conductivity) results in signal increases in both polarization

combinations (Fig. 2A and B, again accounting for size changes observed by DLS, *vide infra*). This signal intensity increase may be attributed to either an increase in the number of oscillators at the droplet surface or to increased lipid ordering of the surface (recall that the PAH methylene groups themselves to not provide SFS signal intensity in PAH-only control experiments in D_2O, as shown in Figure S1.) Fig. 2B also shows a reversal in the intensity ratio between the peaks at 2875 cm^{-1} and 2850 cm^{-1} in the *ppp*-polarized SFS spectra. This outcome indicates a change in lipid conformation at the surface, as a mere increase or decrease in the number of oscillators, without a corresponding change in lipid ordering, would leave the peak intensity ratios the same. This effect is comparable to outcomes from earlier SFS studies comparing oil droplets coated by lipids of varying alkyl tail lengths.[47]

The conformation of PAH in "no added salt" and "100 mM added NaCl" solutions may also play a role in this interaction. According to a study of polyelectrolyte multilayers, which included PAH, PAH became more coiled in solution in response to the presence of various salt solutions.[51] Without salt, the PAH swelled, indicating a more extended conformation in aqueous solutions.[51] Other studies have also documented swelling of PAH in salt-free solutions as well as structural changes of thin films prepared from PAH in response to rinsing with salt-free solutions.[52-53]

Complementary DLS experiments illustrate how the nanodrop size varies upon PAH addition under the conditions of "no salt added" and "100 mM salt added" (Fig. 3A-D). We notice first similar droplet sizes in the absence (Fig. 3A) and presence (Fig. 3C) of salt. Results from replicate experiments shown in the Supporting Information indicate, on occasion, bimodal size distribution, with one population centered at approximately 150 nm (as shown here in the main text) and one at either 350 nm or 500 nm, albeit with smaller intensity. After interaction with a 140

μM PAH solution, the size distributions remain largely unchanged for the case of "no added salt". Yet, in the 100 mM salt cases, the DLS data reveal the presence of a new population in the supermicron size range, having sizes up to 5 μm. The Supporting Information shows these results are observed for up to 8 mM added PAH.

According to the theory of SFS spectroscopy and sum frequency generation (SFG) spectroscopy,[18, 54] decreases in SFS peak intensity observed upon addition of PAH under conditions of "no-salt added" indicates either a loss in the number of oscillators due to lipid removal, a randomization in the orientation of oscillators without a change in the lipid coverage on the droplets, or an ordering of the oscillators in such a way that they destructively interfere with each other (as commonly seen in all-*trans*-configured methylene groups). Given the negligible differences in the relative peak positions seen in Fig. 1, we rule out changes in the number of gauche defects, as those would lead to SFS signal intensity changes only at the methylene stretching frequencies and not across the entire spectrum. A decrease in the number of oscillators at the surface of the oil droplet due to lipid removal would lead to a greater amount of disorder at the interface and a subsequent decrease in the *ssp*- and *ppp*-polarized SFS intensity, as is indeed observed. This Scheme (Scheme 1) is supported by the observation of increased *spp*-polarized SFS intensity shown in Fig. S15 of the Supporting Information, as such a response indicates an uneven lipid arrangement on oil droplets.

Under conditions of 100 mM added salt, we consider charge, which plays an important role in the stability of oil-in-water macroemulsions. For instance, monovalent cations prevent droplets aggregation better than di- or tri-valent cations when the counter-ion is kept the same.[55] Likewise, Kundu et al. reported that coalescence and Ostwald ripening can occur as mechanisms for destabilization and droplet growth in oil-in-water macroemulsions that contain anionic

surfactants.[55] In our present experiments under conditions of 100 mM added salt, PAH may promote the coalescence of nanodroplets, evidenced by the supermicron size fraction seen in the DLS data, by removing lipids from the small droplets. The removal of the lipids provides a destabilizing force by increasing the interfacial tension. During DMPC removal by PAH, hexadecane could also dissolve into the bulk phase and droplets may grow due to a process similar to Ostwald ripening.[56-57]

In the second Scheme (Scheme 2), PAH is bound to the surface of the lipid droplet and does not remove lipids, but instead it disorders the lipids at the interface, resulting in a decrease in SFS intensity in *spp*, *ssp*, and *ppp* polarizations. This Scheme is reminiscent of work reported by Kabalnov et al., who describe a nonionic surfactant-water-decane system whereby the adsorption of a hydrophobically modified naturally occurring polymer causes a change in the curvature of the surfactant leading to an increased rigidity in the system upon polymer addition.[58]

Which Scheme is more likely to occur depends upon the experimental conditions employed in our study. From the DLS data as well as the *ssp*-, *ppp*-, and *spp*-polarized SFS data, Scheme 1 is considered most plausible under high salt conditions, whereas Scheme 2 is more plausible at low salt conditions. The salt concentration dependence of the observations is consistent with increased charge screening under high salt conditions, which decreases the electrical double layer thickness between the polymer and the oil nanodroplet, allowing the PAH to approach the droplet and remove the lipids from the surface.[59-60]

III. B. Low PAH concentration increases SFS signal intensity of DMPC/d-hexadecane nanodroplets even at low [salt] in C-H – but not P-O – stretching region. In various surfactant polymer systems, changing the polymer concentration is known to change the interfacial tension, thus affecting the critical micelle concentration.[61] We therefore lowered the PAH concentration

~tenfold, from 140 μM, discussed in the previous section, to 15 μM at no added salt conditions. Figure 4 shows an increase in *ssp*-polarized SFS intensity at low salt conditions, reminiscent of Scheme 2. This is potentially due to the fact that we have an abundance of oil droplets compared to the concentration of PAH. The *spp* polarization combination is sensitive to the changes in dispersion of lipids on the surface of the oil droplet. If all of the lipids were evenly separated at the surface, and in the presence of uniform lipid coverage, *spp* signal intensity would not be observable.[62-63] If the lipids were distributed non-uniformly, considerable *spp*-polarized SFS signal intensity should be observed.[62-63] Indeed, the *spp*-polarized SFS spectra, which are weak but nevertheless show a decrease in SFS intensity after PAH addition (Figure 5) at 2960 cm^{-1}, support the notion that the lipids are more evenly dispersed under low vs high PAH concentrations, pointing towards Scheme 2.

In contrast to the increases observed in the C-H stretching region for the experiment leading to Figures 4 and 5 (no salt, 15 μM PAH), a PAH concentration of 40 μM causes an SFS signal decrease of DMPC/oil droplets in the PO stretching region (unfortunately, no spectra were taken in the C-H stretching region for that PAH concentration). As shown in Figure 6, the observable features in this spectral region occur near 1070 cm^{-1} (the symmetric CO-O-C stretch) and near 1100 cm^{-1} (the symmetric PO_2^- stretch).[47] As in the case of the C-H stretching region for DMPC in the presence of no salt and 140 μM PAH, the change in the ratio of the SFS intensities at 1070 cm^{-1} and 1100 cm^{-1} is negligible, indicating little to no structural change in the choline headgroup of DMPC when 15 μM PAH interacts with the lipid-coated droplets in the absence of extra salt.

IV. Conclusions. In summary, we have probed several structural aspects of how zwitterionic DMPC lipids adsorbed to oil droplets suspended in D_2O respond to the presence of the common polycation polyallylamine hydrochloride in the presence of low and high salt concentration. We

show that the polycation interactions with the lipids generally results in two distinct outcomes that depend upon salt and PAH concentration, identified here as Scheme 1 (observed under conditions of high salt concentration) and Scheme 2 (observed under conditions of low salt concentration). At 100 mM NaCl and 140 μM PAH, Scheme 1 prevailed, leading to lipid removal by PAH followed by droplet coalescence. Under conditions of no added NaCl and 140 μM PAH, Scheme 2 dominated, which involved PAH surrounding several droplets, thereby changing the lipid orientation but keeping the droplet size constant. Under conditions of no added NaCl and 15 μM PAH, the observations are consistent with Scheme 1, indicating an interplay between NaCl and PAH concentration in determining which Scheme is most likely.

We caution that our results require further investigations into quantifying the size distribution changes that occur under some of the conditions probed here. Moreover, further studies will probe an expanded set of experimental conditions (salt and PAH concentration, lipid and oil composition) in order to determine the scope of our findings. Yet, our present results illustrate that cationic polymers do not always interact in the same fashion with lipid membranes and demonstrate spectroscopic methods to probe those interactions with chemical bond specificity, not only for the alkyl tails, but also the choline headgroup.

Supporting Information Available. Results from PAH controls as well as DLS and SFG replicate experiments are available in the Supporting Information. This information is available free of charge via the Internet at https://pubs.acs.org.

Acknowledgments. This work was supported by the National Science Foundation Center for Chemical Innovation Program, through the Center for Sustainable Nanotechnology (CSN) under Grant No. CHE-1503408. JMT and PEO gratefully acknowledge support through NSF Graduate Research Fellowships. FMG gratefully acknowledges support from a Friedrich Wilhelm Bessel

Prize from the Alexander von Humboldt Foundation. This work is supported by the Julia Jacobi Foundation and the European Research Council (grant number 616305) to SR.

REFERENCES

1. Gole, A.; Murphy, C. J., Polyelectrolyte-Coated Gold Nanorods: Synthesis, Characterization and Immobilization. *Chemistry of Materials* **2005,** *17* (6), 1325-1330.
2. Schmaljohann, D., Thermo- and pH-responsive polymers in drug delivery. *Advanced Drug Delivery Reviews* **2006,** *58* (15), 1655-1670.
3. Carmona-Ribeiro, A.; de Melo Carrasco, L., Cationic Antimicrobial Polymers and Their Assemblies. *International Journal of Molecular Sciences* **2013,** *14* (5), 9906.
4. Bruno, M. M.; Cotella, N. G.; Miras, M. C.; Barbero, C. A., A novel way to maintain resorcinol–formaldehyde porosity during drying: Stabilization of the sol–gel nanostructure using a cationic polyelectrolyte. *Colloids and Surfaces A: Physicochemical and Engineering Aspects* **2010,** *362* (1–3), 28-32.
5. Qiu, T. A.; Torelli, M. D.; Vartanian, A. M.; Rackstraw, N. B.; Jacob, L. M.; Buchman, J. T.; Murphy, C. J.; Hamers, R. J.; Haynes, C. L., Quantification of Free Ligands Present in Colloidal Suspension Reveals Source of Toxic Responses for Polyelectrolyte-wrapped 4-nm-diameter Gold Nanoparticles. *Analytical Chemistry* **2017,** *89*, 1823-1830.
6. Troiano, J. M.; McGeachy, A. C.; Olenick, L. L.; Fang, D.; Liang, D.; Hong, J.; Kuech, T. R.; Caudill, E. R.; Pedersen, J. A.; Cui, Q., et al., Quantifying the Electrostatics of Polycation–Lipid Bilayer Interactions. *J. Am. Chem. Soc.* **2017,** *139*, 5808-5816.
7. McGeachy, A. C.; Caudill, E. R.; Liang, D.; Cui, Q.; Pedersen, J. A.; Geiger, F. M., Counting Charges on Membrane-bound Peptides. *Chem. Sci.* **2018,** *in press, DOI=10.1039/C8SC00804C*.
8. McGeachy, A. C.; Dalchand, N.; Caudill, E. R.; Li, T.; Dogangun, M.; Olenick, L. L.; Chang, H.; Pedersen, J. A.; Geiger, F. M., Interfacial electrostatics of poly (vinylamine hydrochloride), poly (diallyldimethylammonium chloride), poly-l-lysine, and poly-l-arginine interacting with lipid bilayers. *PCCP* **2018,** *in press, DOI=10.1039/C7CP07353D*.
9. Olenick, L. L.; Troiano, J. M.; Vartanian, A. M.; Melby, E. S.; Mensch, A. C.; Zhang, L.; Hong, J.; Qiu, T. A.; Bozich, J. S.; Lohse, S. E., et al., Lipid Corona Formation from Nanoparticle Interactions with Bilayers and Membrane-Specific Biological Outcomes. *ChemRxiv* **2018,** *5512996*.
10. Fischer, D.; Li, Y.; Ahlemeyer, B.; Krieglstein, J.; Kissel, T., In vitro cytotoxicity testing of polycations: influence of polymer structure on cell viability and hemolysis. *Biomaterials* **2003,** *24* (7), 1121-1131.
11. Chew, S. A.; Hacker, M. C.; Saraf, A.; Raphael, R. M.; Kasper, F. K.; Mikos, A. G., Biodegradable Branched Polycationic Polymers with Varying Hydrophilic Spacers for Nonviral Gene Delivery. *Biomacromolecules* **2009,** *10* (9), 2436-2445.
12. Helander, I. M.; Nurmiaho-Lassila, E. L.; Ahvenainen, R.; Rhoades, J.; Roller, S., Chitosan disrupts the barrier properties of the outer membrane of Gram-negative bacteria. *International Journal of Food Microbiology* **2001,** *71* (2–3), 235-244.
13. Fasbender, A.; Zabner, J.; Chillon, M.; Moninger, T. O.; Puga, A. P.; Davidson, B. L.; Welsh, M. J., Complexes of adenovirus with polycationic polymers and cationic lipids increase the efficiency of gene transfer in vitro and in vivo. *J Biol Chem* **1997,** *272* (10), 6479-89.
14. Mecke, A.; Lee, D.-K.; Ramamoorthy, A.; Orr, B. G.; Banaszak Holl, M. M., Synthetic and Natural Polycationic Polymer Nanoparticles Interact Selectively with Fluid-Phase Domains of DMPC Lipid Bilayers. *Langmuir* **2005,** *21* (19), 8588-8590.
15. Hong, S.; Leroueil, P. R.; Janus, E. K.; Peters, J. L.; Kober, M.-M.; Islam, M. T.; Orr, B. G.; Baker, J. R.; Banaszak Holl, M. M., Interaction of Polycationic Polymers with Supported Lipid

Bilayers and Cells: Nanoscale Hole Formation and Enhanced Membrane Permeability. *Bioconjugate Chemistry* **2006,** *17* (3), 728-734.
16. Zhang, Z.-Y.; Smith, B. D., High-Generation Polycationic Dendrimers Are Unusually Effective at Disrupting Anionic Vesicles: Membrane Bending Model. *Bioconjugate Chemistry* **2000,** *11* (6), 805-814.
17. Davydov, D. A.; Romanyuk, A. V.; Rakhnyanskaya, A. A.; Semenyuk, P. I.; Orlov, V. N.; Samoshin, V. V.; Yaroslavov, A. A., Cationic polymer adsorption on bilayer membrane containing anionic and cationic lipids. *Colloid Journal* **2011,** *73* (1), 33-38.
18. Roke, S.; Gonella, G., Nonlinear Light Scattering and Spectroscopy of Particles and Droplets in Liquids. *Annual Review of Physical Chemistry* **2012,** *63* (1), 353-378.
19. Olenick, L. L.; Chase, H. C.; Fu, L.; Zhang, Y.; McGeachy, A. C.; Dogangun, M.; Walter, S. R.; Wang, H.-f.; Geiger, F. M., Single-Component Supported Lipid Bilayers Probed Using Broadband Nonlinear Optics. *PCCP Advance Article DOI 10.1039/C7CP02549A* **2018**.
20. Liu, J.; Conboy, J. C., 1,2-Diacyl-Phosphatidylcholine Flip-Flop Measured Directly by Sum-Frequency Vibrational Spectroscopy. *Biophysical Journal* **2005,** *89* (4), 2522-2532.
21. Anglin, T. C.; Conboy, J. C., Kinetics and Thermodynamics of Flip-Flop in Binary Phospholipid Membranes Measured by Sum-Frequency Vibrational Spectroscopy. *Biochemistry* **2009,** *48* (43), 10220-10234.
22. Anglin, T. C.; Cooper, M. P.; Li, H.; Chandler, K.; Conboy, J. C., Free Energy and Entropy of Activation for Phospholipid Flip-Flop in Planar Supported Lipid Bilayers. *The Journal of Physical Chemistry B* **2010,** *114* (5), 1903-1914.
23. Wu, H.-L.; Tong, Y.; Peng, Q.; Li, N.; Ye, S., Phase transition behaviors of the supported DPPC bilayer investigated by sum frequency generation (SFG) vibrational spectroscopy and atomic force microscopy (AFM). *Physical Chemistry Chemical Physics* **2016,** *18* (3), 1411-1421.
24. Liu, J.; Conboy, J. C., Phase behavior of planar supported lipid membranes composed of cholesterol and 1,2-distearoyl-sn-glycerol-3-phosphocholine examined by sum-frequency vibrational spectroscopy. *Vibrational Spectroscopy* **2009,** *50* (1), 106-115.
25. Liu, J.; Conboy, J. C., Phase Transition of a Single Lipid Bilayer Measured by Sum-Frequency Vibrational Spectroscopy. *Journal of the American Chemical Society* **2004,** *126* (29), 8894-8895.
26. Troiano, J. M.; Olenick, L. L.; Kuech, T. R.; Melby, E. S.; Hu, D.; Lohse, S. E.; Mensch, A. C.; Dogangun, M.; Vartanian, A. M.; Torelli, M. D., et al., Direct Probes of 4 nm Diameter Gold Nanoparticles Interacting with Supported Lipid Bilayers. *The Journal of Physical Chemistry C* **2014,** *119* (1), 534-546.
27. Liu, Y.; Yan, C. Y.; Zhao, X. L.; Eisenthal, K. B., Surface potential of charged liposomes determined by second harmonic generation. *Langmuir* **2001,** *17* (7), 2063-2066.
28. Eisenthal, K. B., Liquid interfaces probed by second-harmonic and sum-frequency spectroscopy. *Chem. Rev.* **1996,** *96* (4), 1343-1360.
29. Eisenthal, K. B., Second Harmonic Spectroscopy of Aqueous Nano- and Microparticle Interfaces *Chem. Rev.* **2006,** *106*, 1462-1477.
30. Troiano, J. M.; Olenick, L. L.; Kuech, T. R.; Melby, E. S.; Hu, D.; Lohse, S. E.; Mensch, A. C.; Dogangun, M.; Vartanian, A. M.; Torelli, M. D., et al., Direct Probes of 4 nm Diameter Gold Nanoparticles Interacting with Supported Lipid Bilayers. *The Journal of Physical Chemistry C* **2015,** *119* (1), 534-546.

31. Rand, D.; Ortiz, V.; Liu, Y.; Derdak, Z.; Wands, J. R.; Tatíček, M.; Rose-Petruck, C., Nanomaterials for X-ray Imaging: Gold Nanoparticle-Enhancement of X-ray Scatter Imaging of Hepatocellular Carcinoma. *Nano letters* **2011,** *11* (7), 2678-2683.
32. Bozich, J. S.; Lohse, S. E.; Torelli, M. D.; Murphy, C. J.; Hamers, R. J.; Klaper, R. D., Surface chemistry, charge and ligand type impact the toxicity of gold nanoparticles to Daphnia magna. *Environmental Science: Nano* **2014,** *1* (3), 260-270.
33. Lohse, S. E.; Eller, J. R.; Sivapalan, S. T.; Plews, M. R.; Murphy, C. J., A Simple Millifluidic Benchtop Reactor System for the High-Throughput Synthesis and Functionalization of Gold Nanoparticles with Different Sizes and Shapes. *ACS Nano* **2013,** *7* (5), 4135-4150.
34. Van Meer, G.; Voelker, D. R.; Feigenson, G. W., Membrane lipids: where they are and how they behave. *Nature Reviews Molecular Cell Biology* **2008,** *9* (2), 112-124.
35. Spector, A. A.; Yorek, M. A., Membrane lipid composition and cellular function. *Journal of Lipid Research* **1985,** *26* (9), 1015-35.
36. Perez-Gil, J.; Weaver, T. E., Pulmonary Surfactant Pathophysiology: Current Models and Open Questions. *Physiology* **2010,** *25* (3), 132-141.
37. Ridgway, N. D., The role of phosphatidylcholine and choline metabolites to cell proliferation and survival. *Critical Reviews in Biochemistry and Molecular Biology* **2013,** *48* (1), 20-38.
38. Leventis, P. A.; Grinstein, S., The Distribution and Function of Phosphatidylserine in Cellular Membranes. *Annual Review of Biophysics* **2010,** *39* (1), 407-427.
39. Chen, Y.; Jena, K. C.; Roke, S., From Hydrophobic to Hydrophilic: The Structure and Density of the Hexadecane Droplet/Alkanol/Water Interface. *The Journal of Physical Chemistry C* **2015,** *119* (31), 17725-17734.
40. Scheu, R.; Rankin, B. M.; Chen, Y.; Jena, K. C.; Ben-Amotz, D.; Roke, S., Charge Asymmetry at Aqueous Hydrophobic Interfaces and Hydration Shells. *Angewandte Chemie International Edition* **2014,** *53* (36), 9560-9563.
41. Smolentsev, N.; Smit, W. J.; Bakker, H. J.; Roke, S., The interfacial structure of water droplets in a hydrophobic liquid. *Nature communications* **2017,** *8* (1-6).
42. Zdrali, E.; Chen, Y.; Okur, H. I.; Wilkins, D. M.; Roke, S., The Molecular Mechanism of Nanodroplet Stability. *ACS Nano* **2017,** *11*, 12111-12120.
43. Mabrey, S.; Sturtevant, J. M., Investigation of phase transitions of lipids and lipid mixtures by sensitivity differential scanning calorimetry. *Proceedings of the National Academy of Sciences* **1976,** *73* (11), 3862-3866.
44. de Aguiar, H. B.; Strader, M. L.; de Beer, A. G. F.; Roke, S., Surface structure of sodium dodecyl sulfate surfactant and oil at the oil-in-water droplet liquid/liquid interface. A manifestation of a nonequilibrium surface state. *J. Phys. Chem. B* **2011,** *115* (12), 2970-2978.
45. de Aguiar, H. B.; Scheu, R.; Jena, K. C.; de Beer, A. G. F.; Roke, S., Comparison of scattering and reflection SFG: a question of phase-matching. *Physical Chemistry Chemical Physics* **2012,** *14* (19), 6826-6832.
46. Scheu, R.; Chen, Y.; Subinya, M.; Roke, S., Stern Layer Formation Induced by Hydrophobic Interactions: A Molecular Level Study. *Journal of the American Chemical Society* **2013,** *135* (51), 19330-19335.
47. Okur, H. I.; Chen, Y.; Smolentsev, N.; Zdrali, E.; Roke, S., Interfacial Structure and Hydration of 3D Lipid Monolayers in Aqueous Solution. *The Journal of Physical Chemistry B* **2017,** *121* (13), 2808-2813.

48. Smolentsev, N.; Lutgebaucks, C.; Okur, H. I.; de, B. A. G. F.; Roke, S., Intermolecular Headgroup Interaction and Hydration as Driving Forces for Lipid Transmembrane Asymmetry. *J Am Chem Soc* **2016,** *138* (12), 4053-60.
49. Chen, Y.; Jena, K. C.; Lutgebaucks, C.; Okur, H. I.; Roke, S., Three Dimensional Nano "Langmuir Trough" for Lipid Studies. *Nano Lett.* **2015**, Ahead of Print.
50. Hensel, J. K.; Carpenter, A. P.; Ciszewski, R. K.; Schabes, B. K.; Kittredge, C. T.; Moore, F. G.; Richmond, G. L., Molecular characterization of water and surfactant AOT at nanoemulsion surfaces. *PNAS* **2017,** *114* (51).
51. Feldötö, Z.; Varga, I.; Blomberg, E., Influence of Salt and Rinsing Protocol on the Structure of PAH/PSS Polyelectrolyte Multilayers. *Langmuir* **2010,** *26* (22), 17048-17057.
52. Ibarz, G.; Dähne, L.; Donath, E.; Möhwald, H., Smart Micro- and Nanocontainers for Storage, Transport, and Release. *Advanced Materials* **2001,** *13* (17), 1324-1327.
53. Fery, A.; Schöler, B.; Cassagneau, T.; Caruso, F., Nanoporous Thin Films Formed by Salt-Induced Structural Changes in Multilayers of Poly(acrylic acid) and Poly(allylamine). *Langmuir* **2001,** *17* (13), 3779-3783.
54. Boyd, R. W., *Nonlinear Optics*. Third ed.; Academic Press: New York, NY, 2008.
55. Kundu, P.; Agrawal, A.; Mateen, H.; Mishra, I. M., Stability of oil-in-water macro-emulsion with anionic surfactant: Effect of electrolytes and temperature. *Chemical Engineering Science* **2013,** *102*, 176-185.
56. Taylor, P., Ostwald ripening in emulsions. *Advances in Colloid and Interface Science* **1998,** *75* (2), 107-163.
57. Thiam, A. R.; Farese, R. V.; Walther, T. C., The Biophysics and Cell Biology of Lipid Droplets. *Nature reviews. Molecular cell biology* **2013,** *14* (12), 775-786.
58. Kabalnov, A.; Lindman, B.; Olsson, U.; Piculell, L.; Thuresson, K.; Wennerström, H., Microemulsions in amphiphilic and polymer-surfactant systems. *Colloid and Polymer Science* **1996,** *274* (4), 297-308.
59. Chattopadhyay, A. K.; Mittal, K. L., *Surfactants in Solution*. Taylor & Francis: 1996.
60. Butt, H. J.; Graf, K.; Kappl, M., *Physics and Chemistry of Interfaces*. Wiley: 2003.
61. Kronberg, B.; Holmberg, K.; Lindman, B., *Surface Chemistry of Surfactants and Polymers*. Wiley: 2014.
62. de Beer, A. G. F.; Roke, S.; Dadap, J. I., Theory of optical second-harmonic and sum-frequency scattering from arbitrarily shaped particles. *J. Opt. Soc. Am. B* **2011,** *28* (6), 1374-1384.
63. Smit, W. J.; Smolentsev, N.; Versluis, J.; Roke, S.; Bakker, H. J., Freezing effects of oil-in-water emulsions studied by sum-frequency scattering spectroscopy. *The Journal of Chemical Physics* **2016,** *145* (4), 044706.

Figure and Scheme Captions.

Figure 1. *ssp*- (A) and *ppp*- (B) polarized sum frequency scattering spectra of DMPC at the d-hexadecane/D_2O interface before (black) and after (gray) interaction with 140 μM PAH in D_2O with no added salt.

Figure 2. *ssp*- (A) and *ppp*- (B) polarized sum frequency scattering spectra of DMPC at the d-hexadecane/D_2O interface before (black) and after (gray) interaction with 140 μM PAH at 100 mM added NaCl in D_2O.

Figure 3. Representative hydrodynamic diameter measurements by DLS of DMPC/oil nanodroplets dispersed in water before (A, C) and after (B, D) interaction with 140 μM PAH under conditions of no added NaCl (A, B) and 100 mM added NaCl (C, D).

Figure 4. *ssp*-polarized sum frequency scattering spectra of DMPC at the d-hexadecane/D_2O interface before (black) and after (gray) interaction with 15 μM PAH in D_2O with no added salt.

Figure 5. *spp*-polarized sum frequency scattering spectra of DMPC at the d-hexadecane/D_2O interface before (black) and after (gray) interaction with 15 μM PAH in D_2O with no added salt.

Figure 6. *ssp*- (A) and *ppp*- (B) polarized SFS spectra in the PO stretching region of DMPC/d-hexadecane droplets dispersed in D_2O before (top spectrum) and after (bottom spectrum) addition of 40 μM PAH in D_2O with no added salt.

Scheme 1. Cartoon representation of the interactions possible between PAH and DMPC-coated oil nanodroplets under conditions of high salt concentration (0.1 M). Gold spheres represent oil droplets. Green shapes represent lipids. Blue shapes represent PAH. Counterions and water molecules omitted for clarity.

Scheme 2. Cartoon representation of the interactions possible between PAH and DMPC oil nanodroplets under conditions of low salt concentration. Gold spheres represent oil droplets. Green shapes represent lipids. Blue shapes represent PAH. Counterions and water molecules omitted for clarity.

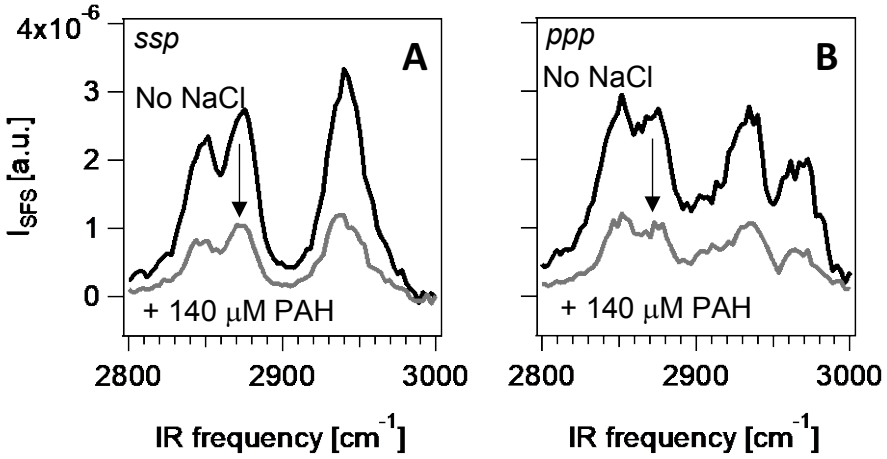
4x10^-6
ssp
A
No NaCl
+ 140 μM PAH
I_SFS [a.u.]
IR frequency [cm^-1]
ppp
B
No NaCl
+ 140 μM PAH
IR frequency [cm^-1]

Figure 1

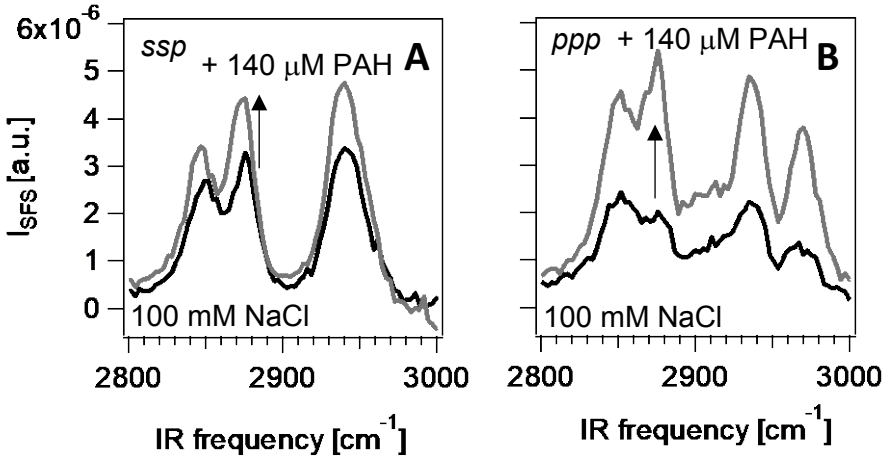
6x10^-6
5
4
3
2
1
0
I_SFS [a.u.]
ssp + 140 μM PAH
A
100 mM NaCl
2800
2900
3000
IR frequency [cm^-1]
ppp + 140 μM PAH
B
100 mM NaCl
2800
2900
3000
IR frequency [cm^-1]

Figure 2

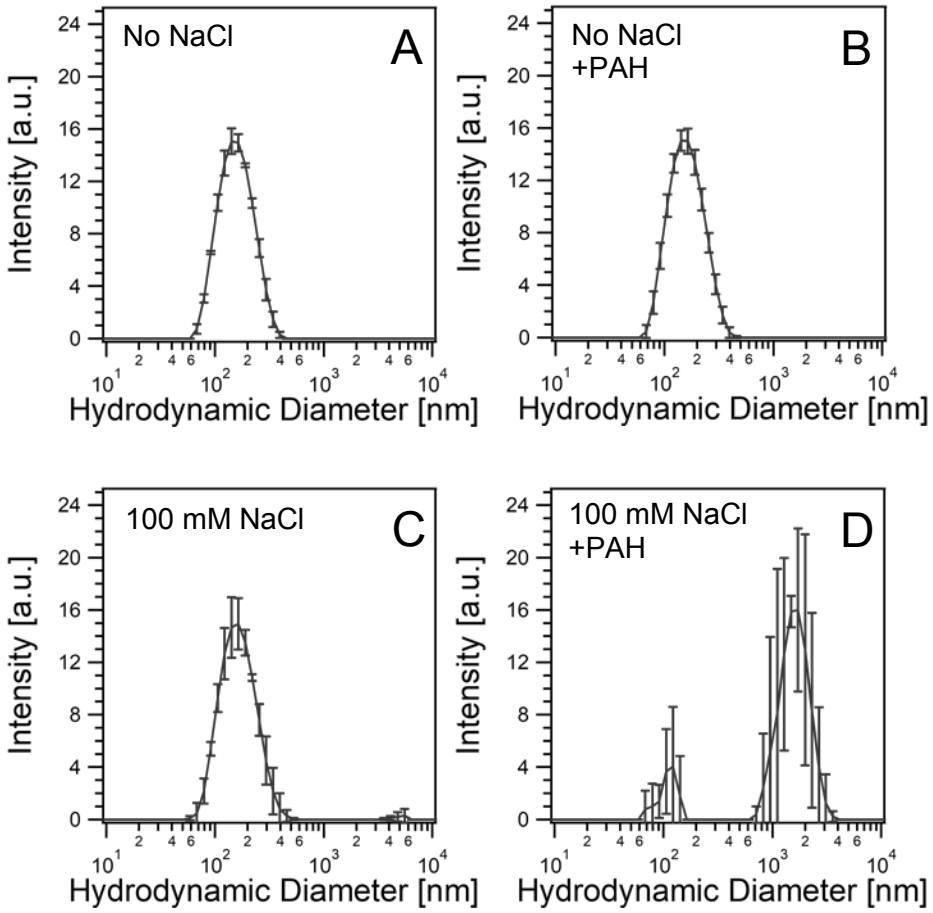
No NaCl
A
No NaCl
+PAH
B
100 mM NaCl
C
100 mM NaCl
+PAH
D
Intensity [a.u.]
Hydrodynamic Diameter [nm]

Figure 3

Page 24

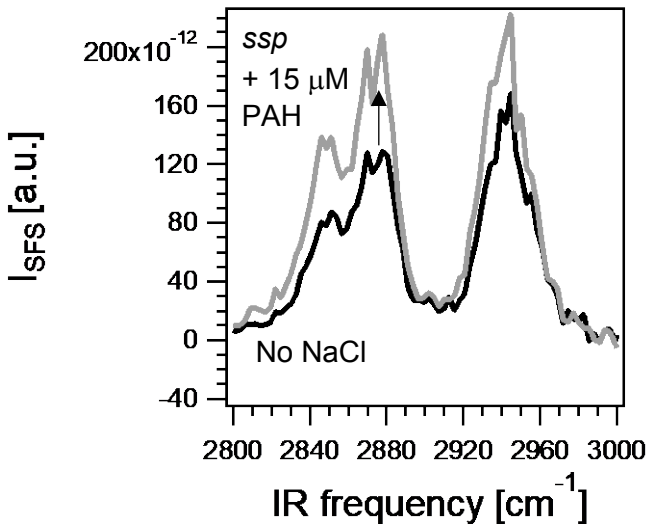

Figure 4

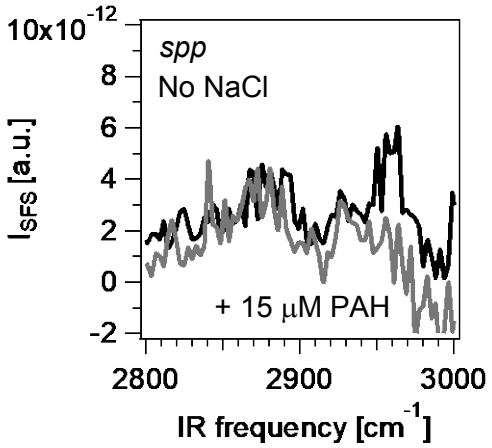
10x10^-12
spp
No NaCl
8
6
4
2
0
-2
I_SFS [a.u.]
+ 15 μM PAH
2800
2900
3000
IR frequency [cm^-1]

Figure 5

Page 26

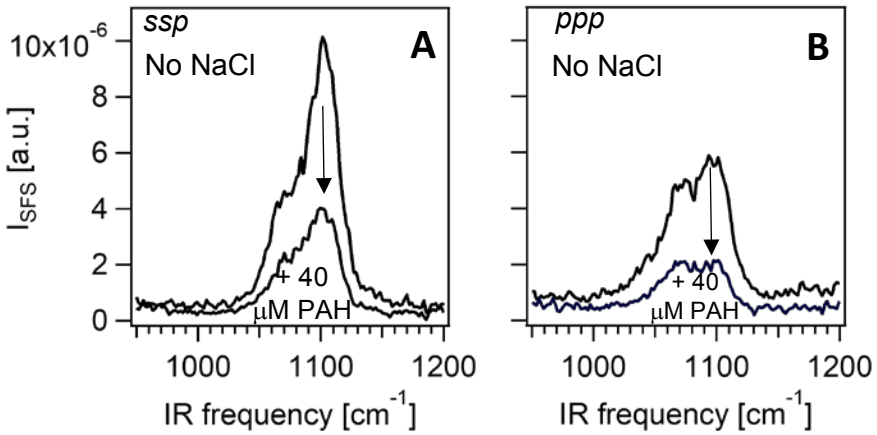

Figure 6

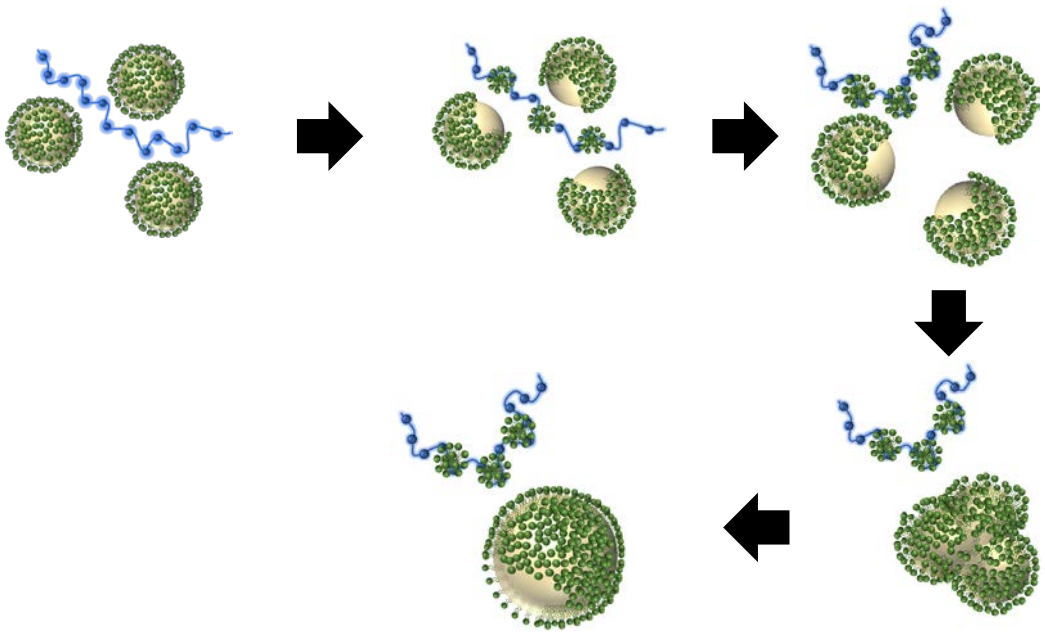

Scheme 1

Page 28

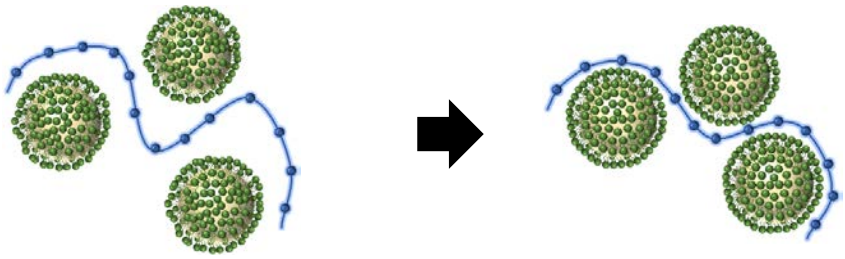

Scheme 2

TOC Graphic